Details on the gravitational-wave emission from rotating gravitational collapse in 3D

Luca Baiotti

Max-Planck-Institut für Gravitationsphysik, Albert-Einstein-Institut, 14476 Golm, Germany

Ian Hawke

School of Mathematics, University of Southampton, Southampton SO17 1BJ, UK

Luciano Rezzolla

Max-Planck-Institut für Gravitationsphysik, Albert-Einstein-Institut, 14476 Golm, Germany
Department of Physics, Louisiana State University, Baton Rouge, LA 70803 USA

Erik Schnetter

Center for Computation & Technology, Louisiana State University, Baton Rouge, LA 70803, USA

E-mail: `baiotti@aei.mpg.de`

Abstract. We here provide details on the numerical study of the gravitational-wave emission from the gravitational collapse to black holes of rotating neutron stars in three dimensions. More specifically, we concentrate on the use of mesh-refined grids, either fixed or progressive, as well as on the use of the excision techniques and of the advantages that result when this is not employed.

1. Introduction

The study of the gravitational collapse of rotating stars to black holes is a cornerstone of any theory of gravity and a long standing problem in General Relativity. Important issues in relativistic astrophysics awaiting clarification, such as the mechanism responsible for γ-ray bursts, may be unveiled with a more detailed understanding of the physics of gravitational collapse in rotating and magnetized stars. Furthermore, the study of gravitational collapse will provide the waveforms and the energetics of one of the most important sources of gravitational radiation.

In our previous work [1, 2, 3], we have described how we can perform accurate three-dimensional (3D) relativistic simulation of such events and extract the weak gravitational signal emitted. Before the results presented in ref. [1], the only work available in the literature on the gravitational radiation produced during the collapse of rotating compact stars to black holes was published almost 20 year ago, with restrictions to axisymmetry and an approximate treatment of the initial conditions [4].

In the present work, after a brief introduction to our code and to the stellar models we have simulated, we give more details on the techniques and the results presented in refs. [2, 3]. We will focus in particular on two technical points: 1) the use of a small amount of numerical dissipation in place of the use of the excision technique to handle the portion of the spacetime inside the black-hole horizon that forms during

the collapse; 2) a comparison between the results obtained when implementing a fixed-mesh-refinement (FMR) strategy rather than a progressive-mesh-refinement (PMR) one.

Hereafter we will use a spacelike signature $(-, +, +, +)$ and a system of units in which $c = G = M_\odot = 1$ (unless explicitly shown otherwise for convenience). Greek indices are taken to run from 0 to 3, Latin indices from 1 to 3 and we adopt the standard convention for the summation over repeated indices.

2. Basic equations and their implementation

The `Whisky` code solves the general relativistic hydrodynamics equations on a 3D numerical grid with Cartesian coordinates [5]. The code has been constructed within the framework of the `Cactus` Computational Toolkit (see refs. [6, 7] for details), and it is developed at the Albert Einstein Institute and at the Louisiana State University. This public domain code provides high-level facilities such as parallelization, input/output, portability on different platforms and several evolution schemes to solve general systems of partial differential equations. Clearly, special attention is dedicated to the solution of the Einstein equations, whose matter-terms in non-vacuum spacetimes are handled by the `Whisky` code.

Stated differently, while the `Cactus` code provides at each time step and on a spatial hypersurface the solution of the Einstein equations

$$G_{\mu\nu} = 8\pi T_{\mu\nu} \,, \tag{1}$$

where $G_{\mu\nu}$ is the Einstein tensor and $T_{\mu\nu}$ is the stress-energy tensor, the `Whisky` code provides the time evolution of the hydrodynamics equations, expressed through the conservation equations for the stress-energy tensor $T^{\mu\nu}$ and for the matter current density J^μ

$$\nabla_\mu T^{\mu\nu} = 0 \,, \qquad \nabla_\mu J^\mu = 0 \,. \tag{2}$$

In what follows we briefly discuss how both the right and the left-hand-side of equations (1) are computed within the coupled `Cactus`/`Whisky` codes.

2.1. Evolution of the field equations

In what follows we give only a brief overview of the system of field equations for the evolution of the field equations, but refer the reader to [8] for more details. Many different formulations of the equations have been proposed throughout the years, starting with the ADM formulation in 1962 [9]. As mentioned in the Introduction, we use the NOK [10] formulation, which is based on the ADM construction and has been further developed in [11].

Details of our particular implementation of the conformal traceless reformulation of the ADM system as proposed by [10, 11, 12] are extensively described in [8, 13] and will not be repeated here. We only mention, however, that this formulation makes use of a conformal decomposition of the three-metric, $\tilde{\gamma}_{ij} = e^{-4\phi}\gamma_{ij}$, and the trace-free part of the extrinsic curvature, $A_{ij} = K_{ij} - \gamma_{ij}K/3$, with the conformal factor ϕ chosen to satisfy $e^{4\phi} = \gamma^{1/3}$, where γ is the determinant of the spatial three-metric γ_{ij}. In this formulation, in addition to the evolution equations for the conformal three-metric $\tilde{\gamma}_j$ and the conformal traceless extrinsic curvature $\tilde{A}_{ij}$, there are evolution equations for the conformal factor ϕ, for the trace of the extrinsic curvature K and for the "conformal connection functions" $\tilde{\Gamma}^i \equiv \tilde{\gamma}^{ij}_{,j}$. We note that although the final mixed, first and second-order, evolution system for the variables $\left\{\phi, K, \tilde{\gamma}_{ij}, \tilde{A}_{ij}, \tilde{\Gamma}^i\right\}$ is not in any immediate sense hyperbolic, there is evidence showing that the formulation is at least equivalent to a hyperbolic system [14, 15, 16]. In the formulation of [11], the auxiliary variables $\tilde{F}_i = -\sum_j \tilde{\gamma}_{ij,j}$ were used instead of the $\tilde{\Gamma}^i$.

2.1.1. Gauge choices The code is designed to handle arbitrary shift and lapse conditions, which can be chosen as appropriate for a given spacetime simulation. More information about the possible families of spacetime slicings which have been tested and used with the present code can be found in [8, 17].

Here, we limit ourselves to recalling details about the specific foliations used in the present evolutions. In particular, we have used hyperbolic K-driver slicing conditions of the form

$$\partial_t \alpha = -f(\alpha)\, \alpha^2 (K - K_0), \tag{3}$$

with $f(\alpha) > 0$ and $K_0 \equiv K(t = 0)$. This is a generalization of many well known slicing conditions. For example, setting $f = 1$ we recover the "harmonic" slicing condition, while, by setting $f = q/\alpha$, with q an integer, we recover the generalized "1+log" slicing condition [18]. In particular, all of the simulations discussed in this paper are done using condition (3) with $f = 2/\alpha$. This choice has been made mostly because of its computational efficiency, but we are aware that "gauge pathologies" could develop with the "1+log" slicings [19, 20].

As spatial gauge, we use one of the "Gamma-driver" shift conditions proposed in [17] (see also [13]), that essentially act so as to drive the $\tilde{\Gamma}^i$ to be constant. In this respect, the "Gamma-driver" shift conditions are similar to the "Gamma-freezing" condition $\partial_t \tilde{\Gamma}^k = 0$, which, in turn, is closely related to the well-known minimal distortion shift condition [21]. The differences between these two conditions involve the Christoffel symbols and are basically due to the fact that the minimal distortion condition is covariant, while the Gamma-freezing condition is not.

In particular, all the results reported here have been obtained using the hyperbolic Gamma-driver condition,

$$\partial_t^2 \beta^i = F\, \partial_t \tilde{\Gamma}^i - \eta\, \partial_t \beta^i, \tag{4}$$

where F and η are, in general, positive functions of space and time. For the hyperbolic Gamma-driver conditions it is crucial to add a dissipation term with coefficient η to avoid strong oscillations in the shift. Experience has shown that by tuning the value of this dissipation coefficient it is possible to almost freeze the evolution of the system at late times. We typically choose $F = 3/4$ and $\eta = 3$ and do not vary them in time.

The singularity-avoiding properties of the above gauge choices have proved equally good both when using excision, as we did in refs. [1] and [2], and when not using excision. In this latter case, the addition of a small dissipation in the metric and gauge terms is necessary to obtain long-term stable evolutions [3] (a more extended discussion of this will be presented in Section 5). In the absence of an excised region of spacetime, the gauge choices (4) are essential to "freeze" the evolution in those regions of the computational domain inside the apparent horizon (AH), where the metric functions experience the growth of very large gradients.

2.2. Evolution of the hydrodynamics equations

An important feature of the `Whisky` code is the implementation of a *conservative formulation* of the hydrodynamics equations [22, 23, 24], in which the set of equations (2) is written in a hyperbolic, first-order and flux-conservative form of the type

$$\partial_t \mathbf{q} + \partial_i \mathbf{f}^{(i)}(\mathbf{q}) = \mathbf{s}(\mathbf{q})\,, \tag{5}$$

where $\mathbf{f}^{(i)}(\mathbf{q})$ and $\mathbf{s}(\mathbf{q})$ are the flux-vectors and source terms, respectively [25]. Note that the right-hand side (the source terms) depends only on the metric, and its first derivatives, and on the stress-energy tensor. Furthermore, while the system (5) is not strictly hyperbolic, strong hyperbolicity is recovered in a flat spacetime, where $\mathbf{s}(\mathbf{q}) = 0$.

Additional details of the formulation we use for the hydrodynamics equations can be found in ref. [25]. We stress that an important feature of this formulation is that it has allowed to extend to a general relativistic context the powerful numerical methods developed in classical hydrodynamics, in particular High-Resolution Shock-Capturing schemes based on exact [26, 27, 28] or approximate Riemann solvers (see ref. [25] for a detailed bibliography). Such schemes are essential for a correct representation of shocks, whose presence is expected in several astrophysical scenarios.

3. Perturbative Wave Extraction

Although several different methods are possible for the extraction of the gravitational-radiation content in numerical spacetimes, we have adopted a gauge-invariant approach in which the spacetime is matched with the non-spherical perturbations of a Schwarzschild black hole (see refs. [29, 30, 31] for applications to Cartesian coordinates grids). In practice, a set of "observers" is placed on 2-spheres of fixed coordinate radius, where they extract the gauge-invariant, even $\Psi_{\ell m}^{(e)}$ and odd-parity $Q_{\ell m}^{(o)}$ metric perturbations [32]. Here ℓ, m are the indices of the angular decomposition and we usually compute modes up to $\ell = 5$ with $m = 0$; modes with $m \neq 0$ are essentially zero because of the high degree of axisymmetry in the collapse. Validations of this approach in vacuum spacetimes can be found in refs. [31, 33, 34], while its use with matter sources has been reported in [35].

Using the extracted gauge-invariant quantities it is also possible to calculate the transverse traceless (TT) gravitational-wave amplitudes in the two polarizations h_+ and $h_\times$ as [36]

$$h_+ - \mathrm{i}h_\times = \frac{1}{\sqrt{2}r} \sum_{\ell,m} \left(Q_{\ell m}^+ - \mathrm{i} \int_{-\infty}^t Q_{\ell m}^\times(t')dt' \right) {}_{-2}Y^{\ell m}, \tag{6}$$

where ${}_{-2}Y^{\ell m}$ is the $s = -2$ spin-weighted spherical harmonic and the even and odd-parity perturbations $Q_{\ell m}^+$ and $Q_{\ell m}^\times$ are defined as

$$Q_{\ell m}^+ \equiv \sqrt{\frac{2(\ell + 2)!}{(\ell - 2)!}} \, \Psi_{\ell m}^{(e)}, \qquad Q_{\ell m}^\times \equiv \sqrt{\frac{2(\ell + 2)!}{(\ell - 2)!}} \, Q_{\ell m}^{(o)}. \tag{7}$$

Because of the small amplitude of higher-order modes, the TT wave amplitudes can be simply expressed as $h_+ \simeq h_+(Q_{20}^+, Q_{40}^+), Q_{20}^+ \gg Q_{40}^+$, and $h_\times \simeq h_\times(Q_{30}^\times, Q_{50}^\times)$, where $Q_{30}^\times \gg Q_{50}^\times$. The emitted power is then computed as

$$\frac{dE}{dt} = \frac{1}{32\pi} \sum_{\ell,m} \left(\left| \frac{dQ_{\ell m}^+}{dt} \right|^2 + \left| Q_{\ell m}^\times \right|^2 \right), \tag{8}$$

and the emitted energy is its integral:

$$\Delta E \equiv \int \frac{dE(t')}{dt} dt'. \tag{9}$$

4. Initial stellar models

As mentioned earlier, this paper is specially dedicated to study the gravitational collapse of uniformly rotating supramassive relativistic stars that have become unstable to axisymmetric perturbations. Given equilibrium models of gravitational mass M and central energy density e_c along a sequence of fixed angular momentum or fixed rest mass, the Friedman, Ipser & Sorkin criterion $\partial M/\partial e_c = 0$ [37] can be used to locate the exact onset of the *secular* instability to axisymmetric collapse. The onset of the *dynamical* instability to collapse is located near that of the secular instability but at somewhat larger central energy densities. Unfortunately, no simple criterion exists to determine this location, but the expectation mentioned above has been confirmed by the simulations performed here and by those discussed in [38]. Note that, in the absence of viscosity or strong magnetic fields, the star is not constrained to rotate uniformly after the onset of the secular instability and could develop differential rotation. In a realistic neutron star, however, viscosity or intense magnetic fields are likely to enforce a uniform rotation and cause the star to collapse soon after it passes the secular instability limit.

For simplicity, we have focused on initial models constructed with a polytropic EOS $p = K\rho^\Gamma$, choosing $\Gamma = 2$ and polytropic constant $K_{\mathrm{ID}} = 100$ to produce stellar models that are, at least
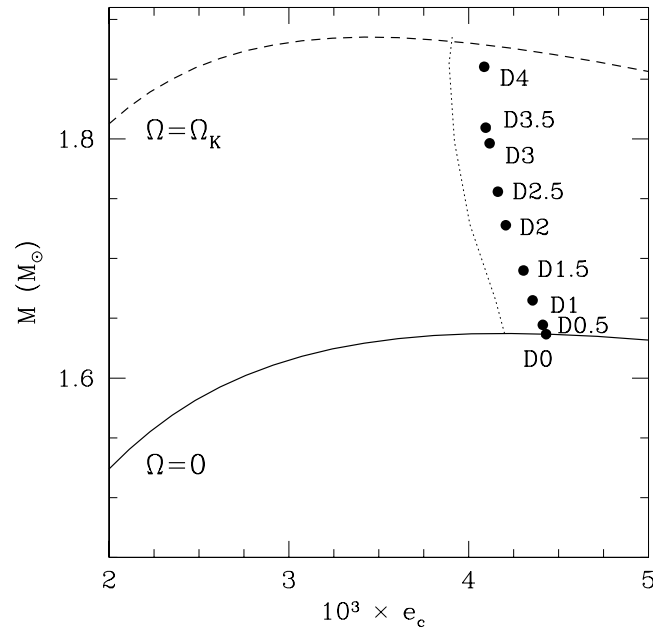
Figure 1. Gravitational mass shown as a function of the central energy density for equilibrium models constructed with the polytropic EOS, for $\Gamma = 2$ and polytropic constant $K_{\rm ID} = 100$. The solid, dashed and dotted lines correspond to the sequence of non-rotating models, the sequence of models rotating at the mass-shedding limit $\Omega_{\rm K}$ and the sequence of models that are at the onset of the secular instability to axisymmetric perturbations. Also shown are the dynamically unstable (filled circles) initial models used in the collapse simulations.

qualitatively, representative of what is expected from observations of neutron stars. More specifically, we have first identified nine models having polar-to-equatorial axes ratio in the interval 0.65–1.0 and lying on the line defining the onset of the secular instability (the dotted line in Fig.1). We have then used these fiducial models to determine those that are dynamically unstable and therefore suitable for ours evolutions. In practice, these unstable stars are obtained as those having the same axis ratio as those that are secularly unstable, but with a central energy density which is larger of about 5%.

All of the models selected in this way have indeed been found to be dynamically unstable [1] and we have indicated them as D0, D1, D1.5, D2...D4 (see Fig.1 and Table 1), following with same convention introduced in ref. [1].

Figure 1 shows the gravitational mass as a function of the central energy density for equilibrium models constructed with the chosen polytropic EOS. The solid, dashed and dotted lines correspond respectively to: the sequence of non-rotating models, the sequence of models rotating at the mass-shedding limit $\Omega_{\rm K}$ and the sequence of models that are at the onset of the secular instability to axisymmetric perturbations. The dynamically unstable initial models used in the collapse simulations are shown as filled circles.

Table 1 summarizes the main equilibrium properties of the initial models. The circumferential equatorial radius is denoted as R_e, while Ω is the angular velocity with respect to an inertial observer at infinity, and r_p/r_e is the ratio of the polar to equatorial coordinate radii. Other quantities shown are the central rest-mass density ρ_c, the ratio of the angular momentum J to the square of the gravitational mass M, and the ratio of rotational kinetic energy to gravitational binding energy $T/|W|$.

Table 1. Equilibrium properties of the initial stellar models. The different columns refer respectively to: the central rest-mass density ρ_c, the ratio of the polar to equatorial coordinate radii r_p/r_e, the gravitational mass M, the circumferential equatorial radius R_e, the angular velocity Ω, the ratio J/M^2 where J is the angular momentum, the ratio of rotational kinetic energy to gravitational binding energy $T/|W|$. All models have been computed with a polytropic EOS with $K_{\rm ID} = 100$ and $\Gamma = 2$.

Model	$\rho_c^{\dagger}$	r_p/r_e	M	R_e	$\Omega^{\ddagger}$	J/M^2	$T/|W|^{\ddagger}$
D0	3.325	1.00	1.636	7.54	0.00	0.00	0.00
D0.5	3.314	0.99	1.644	7.59	0.92	0.108	0.32
D1	3.280	0.95	1.665	7.74	1.73	0.206	1.16
D1.5	3.249	0.91	1.690	7.91	5.76	0.281	2.13
D2	3.189	0.85	1.728	8.21	2.88	0.362	3.52
D2.5	3.162	0.81	1.756	8.43	3.20	0.410	4.48
D3	3.134	0.75	1.797	8.80	3.55	0.468	5.79
D3.5	3.121	0.73	1.810	8.93	3.65	0.485	6.20
D4	3.116	0.65	1.861	9.65	3.95	0.543	7.67

$\dagger$ $\times 10^{-3}$
$\ddagger$ $\times 10^{-2}$

5. Excise or not?

The use of the excision technique was essential in ref. [1] for studying the dynamics of the collapse with uniform grids, because these, combined with the computational resources available at that time, had forced us to use outer boundaries close to the stellar surface and a relatively coarse resolution. Such a resolution was sufficient to describe accurately the dynamics of the matter and of the horizons but also required the use of excision if the simulation had to be carried out beyond the horizon formation.

As an important improvement on the approach discussed above, the code was extended so as to allow for the solution of both the fields and hydrodynamics equations on non-uniform grids using a "box-in-box" mesh refinement strategy [39] (see Fig. 2). This change introduces two important advantages: firstly, it reduces the influence of inaccurate boundary conditions at the outer boundaries which can be moved far from the central source; secondly, it allows for the wave zone to be included in the computational domain and thus for the extraction of important information about the gravitational wave emission produced during the collapse.

In practice, we have adopted a Berger–Oliger prescription for the refinement of meshes on different levels [40] and used the numerical infrastructure described in [39], i.e., the `Carpet` mesh refinement driver for `Cactus` (see [41] for details). In addition to this, in ref. [2] we had also used a simplified form of adaptivity in which new refined levels are added at predefined positions during the evolution (see ref. [42] for details and tests). This progressive mesh refinement, which allows to use much less computational resources, was the key improvement to our previous code [1] and allowed to extract, for the first time in 3D calculations, the gravitational waveform from the collapse to a rotating black hole.

A significant outcome of the calculations using PMR was that applying excision only to matter variables led to slightly longer simulations, but that these could be extended considerably by adding a small amount of dissipation on the metric and gauge variables. More specifically, we use an artificial dissipation of the Kreiss–Oliger type [43] on the right hand sides of the evolution equations for the spacetime variables and the gauge quantities. This is needed mostly because all the field variables develop very steep gradients in the region inside the AH. Under these conditions, small high-frequency oscillations (either produced by finite-differencing errors or by small reflections across the refinement or outer boundaries) can easily be amplified, leave the region inside the AH and rapidly destroy the solution. In practice, for any time-evolved quantity u, the right-hand-side of the corresponding evolution equation
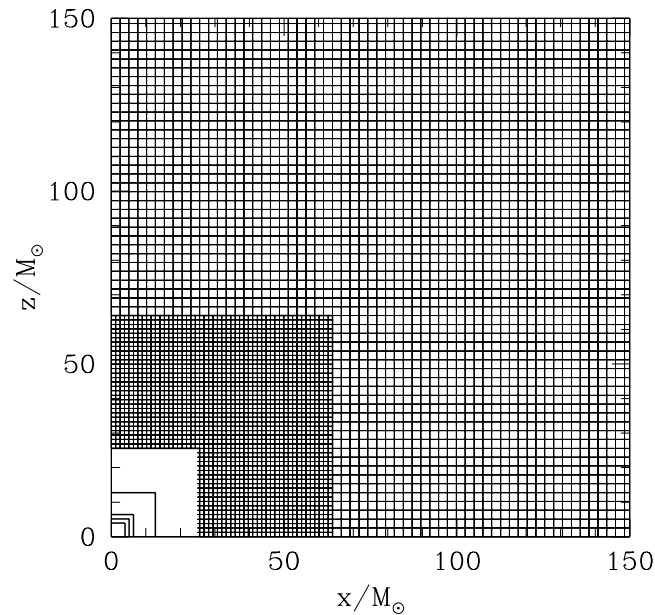
Figure 2. Grid structure: 2-dimensional slices orthogonal to one of the axes of the refined grid used for the evolutions described in the text. The outermost grid extends actually to $\sim 300 M_\odot$ in the simulations, but here, in order to make the refined grids visible in the figure, the image has been restricted to $x = z = 150 M_\odot$.

is modified with the introduction of a term of the type $\mathcal{L}_{\mathrm{diss}}(u) = -\varepsilon h^3 \partial_i^4 u$, where h is the grid spacing, and ε is the dissipation coefficient, which is allowed to vary in space.

We have experimented with configurations in which the coefficient was either constant over the whole domain or larger for the grid points inside the AH. We noticed no significant difference between these two cases. Much more sensitive is instead the choice of the *value* of ε. In the simulations reported here, the employed values of ε are between 0.0075 and 0.02. For each initial model, two values of ε can be determined, such that for values smaller than the smaller of the two the dissipation is not strong enough to cure the instability, and such that for values larger than the larger of the two the solution is different from the one obtained without dissipation (overdissipation). Such differences in the solution cannot be seen in the dynamics of the matter or of the horizons, but only in the very sensitive waveforms.

The use of numerical dissipation stops the growth of the metric functions, which, instead of growing more and more while approaching the singularity, stabilise to a stationary state. Outside the horizon, the spacetime is practically identical to the one obtained without dissipation and the dynamics of the horizon itself is the same as in the case in which excision was performed (up to when the latter data are available). On the contrary, the metric inside the horizon is rather far from being a solution of the Einstein equations, but this does not influence the outside spacetime, as shown also in Fig. 2 of ref. [3]. Note that no dissipation is added to the evolution of any matter variable.

The introduction of this small dissipation makes the use of the excision technique for matter variables quite irrelevant. Indeed, once the matter is within the apparent horizon, it ceases to have any influence on the evolution even numerically. As the matter collapses and concentrates over a very few grid points (and ultimately on only one), in fact, the high accuracy of the HRSC methods is able to conserve the rest mass to very high precision with a loss of less than 0.2% up to when the narrowly peaked rest-mass density distribution is diffused as a result of the poorly resolved gradients (*cf.* Fig. 1 of [3]).
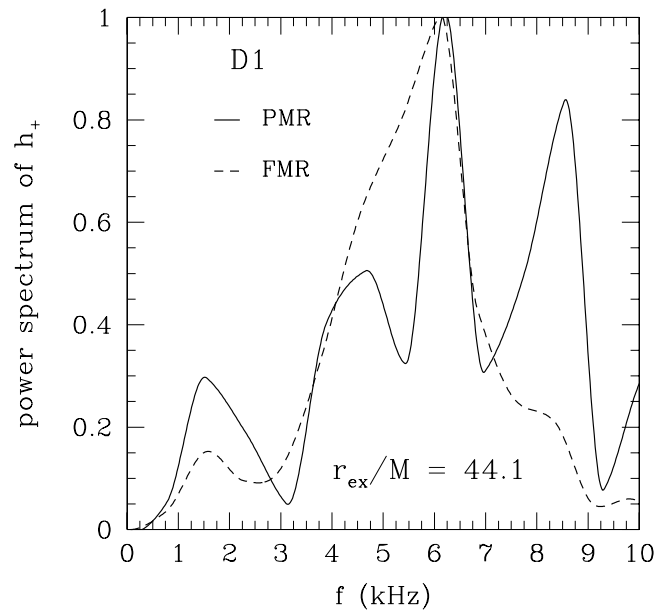
Figure 3. Power spectral density of h_+ with PMR and FMR. The main peak frequencies are the same.

6. Progressive *vs* Fixed Mesh-Refinements

As larger computational resources have recently become available, we have also been able to assess the influence of a progressive mesh refinement on the evolution of the matter and on the waveforms produced. In practice, the set of refinement levels is setup initially to match the final one discussed in ref. [2] and not modified further during the evolution. In particular, our grids are set as follows: the innermost grid has a resolution of $\Delta x = 0.04\,M_\odot$ and other grids are factors of two less resolved, up to the outermost, which has a resolution of $\Delta x = 2.56\,M_\odot$ and extends up to $\sim 307\,M_\odot \simeq 40\,R_*$ (see Fig. 2).

While computationally more expensive (higher resolution is used also when not strictly necessary), this approach also suppresses the small truncation error introduced at the time when a new refinement level is added. Indeed, from the analysis of a large set of tests we have found that the activation of refined grids during the evolution, while leaving the evolution of the matter and of the horizon essentially unaltered, causes differences in the waveforms, whose amplitude is intrinsically very small.

In Fig. 3 we show the power spectral density of the "plus" polarization h_+ as obtained with progressive (continuous line) and fixed (dashed line) mesh refinements. Note that the energies and frequencies of the main peaks coincide indicating that the fundamental features of the signal are unaltered when passing from PMR to FMR. In addition, also the other frequencies at which the power spectrum has local maxima coincide in the two cases, although the amplitudes are different, especially at higher frequencies. In particular, the PMR data contains a significantly larger power at higher frequencies; we associate this additional power to the activation of the additional refined grids.

As a final remark, we show in Fig. 4 the lowest-order gauge-invariant quantity Q_{20} as obtained from simulations using FMR at three different resolutions (i.e., $2\Delta x$, Δx and $\Delta x/2$). The three results for the waveforms are well superposed, in particular those for the two highest resolutions, indicating that the convergent regime has been reached also for the waveforms. The frequencies and the carried energies computed in the three cases differ by less than 10%.
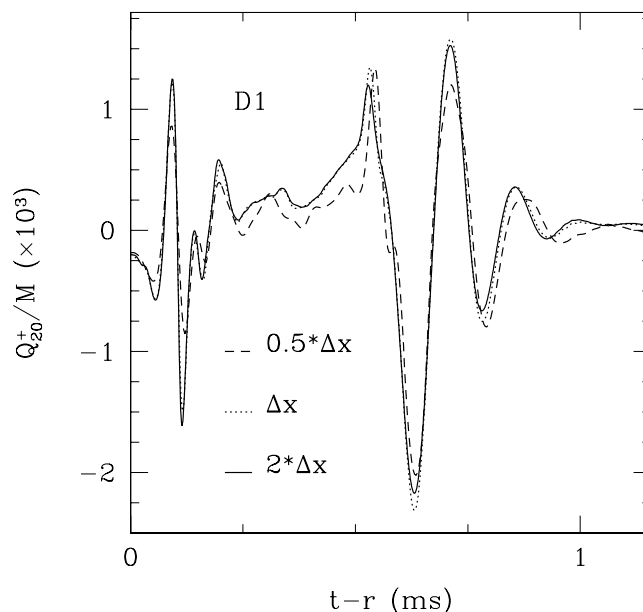
Figure 4. Comparison of the waveforms for Q_{20} for three resolutions.

References
[1] Baiotti L, Hawke I, Montero P J, Löffler F, Rezzolla L, Stergioulas N, Font J A and Seidel E 2005 *Phys. Rev.* D **71** 024035 (*Preprint* gr-qc/0403029)
[2] Baiotti L, Hawke I, Rezzolla L and Schnetter E 2005 *Phys. Rev. Lett.* **94** 131101 (*Preprint* gr-qc/0503016)
[3] Baiotti L and Rezzolla L 2006 *Phys. Rev. Lett.* **97** 141101
[4] Stark R F and Piran T 1985 *Phys. Rev. Lett.* **55** 891
[5] Baiotti L, Hawke I, Montero P and Rezzolla L 2003 in R Capuzzo-Dolcetta, ed, *Computational Astrophysics in Italy: Methods and Tools* (Trieste: Mem. Soc. Astron. It. Suppl.) vol 1 p 210
[6] Goodale T, Allen G, Lanfermann G, Massó J, Radke T, Seidel E and Shalf J 2003 in *Vector and Parallel Processing – VECPAR'2002, 5th International Conference, Lecture Notes in Computer Science* (Berlin: Springer)
[7] Cactus Computational Toolkit home page URL http://www.cactuscode.org/
[8] Alcubierre M, Brügmann B, Dramlitsch T, Font J A, Papadopoulos P, Seidel E, Stergioulas N and Takahashi R 2000 *Phys. Rev.* D **62** 044034 (*Preprint* gr-qc/0003071)
[9] Arnowitt R, Deser S and Misner C W 1962 in L Witten, ed, *Gravitation: An introduction to current research* (New York: John Wiley) pp 227–265 (*Preprint* gr-qc/0405109)
[10] Nakamura T, Oohara K and Kojima Y 1987 *Prog. Theor. Phys. Suppl.* **90** 1–218
[11] Shibata M and Nakamura T 1995 *Phys. Rev.* D **52** 5428
[12] Baumgarte T W and Shapiro S L 1999 *Phys. Rev.* D **59** 024007 (*Preprint* gr-qc/9810065)
[13] Alcubierre M, Brügmann B, Diener P, Koppitz M, Pollney D, Seidel E and Takahashi R 2003 *Phys. Rev.* D **67** 084023 (*Preprint* gr-qc/0206072)
[14] Sarbach O, Calabrese G, Pullin J and Tiglio M 2002 *Phys. Rev.* D **66** 064002 (*Preprint* gr-qc/0205064)
[15] Bona C, Ledvinka T, Palenzuela C and Zacek M 2004 *Phys. Rev.* D **69** 064036 (*Preprint* gr-qc/0307067)
[16] Nagy G, Ortiz O E and Reula O A 2004 *Phys. Rev.* D **70** 044012 (*Preprint* gr-qc/0402123)

[17] Alcubierre M, Brügmann B, Pollney D, Seidel E and Takahashi R 2001 *Phys. Rev.* D **64** 061501(R) (*Preprint* gr-qc/0104020)

[18] Bona C, Massó J, Seidel E and Stela J 1995 *Phys. Rev. Lett.* **75** 600–603 (*Preprint* gr-qc/9412071)

[19] Alcubierre M 1997 *Phys. Rev.* D **55** 5981–5991 (*Preprint* gr-qc/9609015)

[20] Alcubierre M and Massó J 1998 *Phys. Rev.* D **57**(8) R4511–R4515 (*Preprint* gr-qc/9709024)

[21] Smarr L and York J W 1978 *Phys. Rev.* D **17**(10) 2529–2552

[22] Martí J M, Ibáñez J M and Miralles J M 1991 *Phys. Rev.* D **43** 3794

[23] Banyuls F, Font J A, Ibáñez J M, Martí J M and Miralles J A 1997 *Astrophys. J.* **476** 221

[24] Ibáñez J, Aloy M, Font J, Martí J, Miralles J and Pons J 2001 in E Toro, ed, *Godunov methods: theory and applications* (New York: Kluwer Academic/Plenum Publishers)

[25] Font J A 2003 *Living Rev. Relativity* **6** 4 URL http://www.livingreviews.org/Articles/lrr-2003-4

[26] Martí J M and Müller E 1999 *Living Rev. Relativity* **2** 3 (*Preprint* astro-ph/9906333) URL http://www.livingreviews.org/lrr-1999-3

[27] Rezzolla L and Zanotti O 2001 *Journ. of Fluid Mech.* **449** 395

[28] Rezzolla L, Zanotti O and Pons J A 2003 *Journ. of Fluid Mech.* **479** 199

[29] Allen G, Camarda K and Seidel E 1998 3D black hole spectroscopy: Determining waveforms from 3D excited black holes (*Preprint* gr-qc/9806036)

[30] Rupright M E, Abrahams A M and Rezzolla L 1998 *Phys. Rev.* D **58** 044005

[31] Camarda K and Seidel E 1999 *Phys. Rev.* D **59** 064019 (*Preprint* gr-qc/9805099)

[32] Moncrief V 1974 *Annals of Physics* **88** 323–342

[33] Rezzolla L, Abrahams A M, Matzner R A, Rupright M E and Shapiro S L 1999 *Phys. Rev.* D **59** 064001 (*Preprint* gr-qc/9807047)

[34] Baker J, Brandt S R, Campanelli M, Lousto C O, Seidel E and Takahashi R 2000 *Phys. Rev.* D **62** 127701

[35] Font J A, Goodale T, Iyer S, Miller M, Rezzolla L, Seidel E, Stergioulas N, Suen W M and Tobias M 2002 *Phys. Rev.* D **65** 084024 (*Preprint* gr-qc/0110047)

[36] Nagar A and Rezzolla L 2005 *Class. and Quantum Grav.* **22**(16) R167–R192 URL http://stacks.iop.org/0264-9381/22/R167

[37] Friedman J L, Ipser J R and Sorkin R D 1988 *Astrophys. J.* **325** 722–724

[38] Shibata M, Baumgarte T W and Shapiro S L 2000 *Phys. Rev.* D **61** 044012 gr-qc/9911308

[39] Schnetter E, Hawley S H and Hawke I 2004 *Class. Quantum Grav.* **21**(6) 1465–1488 (*Preprint* gr-qc/0310042)

[40] Berger M J and Oliger J 1984 *J. Comput. Phys.* **53** 484–512

[41] Mesh Refinement with Carpet URL http://www.carpetcode.org/

[42] Ott C D to be submitted *Multidimensional Simulations of Stellar Iron Core Collapse in General Relativity and Newtonian Gravity — Gravitational Wave Emission in Core-Collapse Supernovae* Ph.D. thesis Universität Potsdam

[43] Kreiss H O and Oliger J 1973 *Methods for the approximate solution of time dependent problems* vol 10 (World Meteorological Organization, International Council of Scientic Unions)